Modeling Energy Dissipation and Deformation in a Tumbling Defunct Satellite Using a Finite Element Method

Ryotaro Sakamoto and Daniel J. Scheeres
University of Colorado Boulder
3775 Dicovery Dr, Boulder, CO 80309

ABSTRACT

The combination of finite element methods and rigid body theory are used to model energy dissipation in defunct satellites placed in a complex rotation state by the YORP effect. To determine a model for accurate yet efficient modeling of energy dissipation, we evaluate a hysteresis approach based on the Bouc-Wen model. This analysis will contribute to the precise modeling of non-uniformly rotating debris and defunct satellites.

1. INTRODUCTION

Solar radiation pressure leading to the Yarkovsky-O'Keefe-Radizievskii-Paddack (YORP) effect is considered to be one cause of changes in the rotational states of defunct geosynchronous earth orbit (GEO) satellites, in some cases taking them from uniform rotation to tumbling. For example, the transition of the rotational rates has been predicted and observed in the GOES 8 satellite [1]. This effect does not only affect defunct satellites, as the rotational rates of small asteroids are also changed by the YORP effect [2]. It has been predicted that internal energy dissipation is also an important component in the evolution of satellite spin states. Ideally, the kinetic energy is conserved without any additional torque for rigid body dynamics. In real life, friction between structural components or sloshing of internal liquid systems are considered as reasons for dissipation in space [3]. As a tumbling spacecraft loses energy, the state of the rotational rate approaches rotation along its maximum momentum inertia. In terms of the three-dimensional dynamics, rotational rate along its maximum momentum inertia goes to a value based on minimum energy theory with the other rotational rates going to zero. One goal of this work is to find the relationship between energy dissipation and rotational rate for spinning defunct satellites and debris in general. In this research, we focus on the deformation of the satellite, which is one aspect of the energy dissipation. Deformational calculations are conducted using a Finite Element Method (FEM) analysis of a flexible satellite model. The detailed FEM model captures the behavior of internal variations of the position of the nodes, their velocity and the total system kinetic energy. Time varying accelerations are applied using a tumbling satellite model. By combining the finite element analysis and rigid body dynamics, including the deformation effects, the energy transition in the spin state is modeled and revealed. Our three-dimensional model is composed of a simple solar array and body component using a finite element model. One model has a solar array and body component. Another model has two symmetric panels. To evaluate the energy transition, the absorbed energy is compared across different spin rates. As a mathematical approach, the FEM dynamics and nonlinear hysteretic dynamics based on the Bouc-Wen model are considered. The Bouc-Wen model has been widely used to show the nonlinear hysteretic systems and its energy dissipation. The Bouc-Wen model is a nonlinear differential equation which describes the dependence of the output while introducing an extra state variable [4]. Using appropriate parameters in the Bouc-Wen model, it allows us to describe a variety of hysteretic behavior. At first, dynamics which has FEM and the Bouc-Wen model is tumbled with acceleration matrix. Then elastic and hysteretic forces are evaluated. Based on the total restoring force, a fitting function is calculated with Fast Fourier Transform (FFT) with dynamics is transformed from the multiple node system into a simplified system. Finally, using the fitting function as an excitation force for the simple system, a hysteresis plot is depicted and absorbed energy is compared. These simulations will be compared with the observation data for the tumbling satellite GOES-8 [1] to develop estimates of what appropriate level of dissipation should be used in our simulations for this particular spacecraft.
The organization of this paper is as follows. In Section 2, the FEM and analysis model are reviewed. Using the FEM model, a tumbling simulation is considered in Section 3. The hysteresis approach to investigate energy loss using FEM and the Bouc-Wen mdoel is explained in Section 4. Finally, a summary of findings is shown in Section 5.

2. THREE DIMENSIONAL MODEL

In this section, we discuss the basis of the Finite Element Method (FEM) briefly. And two analysis models are developed with FEM, which are applied in this research. FEM has advantages as a tool to evaluate the material properties and their energy loss effectively [5]. It calculates the displacements of the structural nodes from their original positions, and analyzes the effect of the geometry on damping.

2.1 Finite element method

Fig.1 shows one element which is used to construct two models. Each element has two nodes. L indicates the length of an element, the circled number is the node number. Node coordinate matrices are also defined following equations (1) and (2). The node coordinate has three components, X, Y, and Z. Also, the degrees of freedom are defined by six components, which are X, Y, Z directions, and the angles of between them.

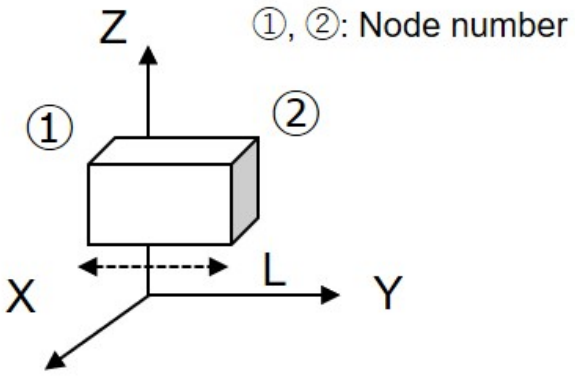

Fig. 1: One element and node number

$$Node\ Coordinate = \left[\begin{array}{ccc} X & Y & Z \end{array} \right] \tag{1}$$

$$Node\ Coordinate\ Matrix = \left[\begin{array}{c} Node_{①} \\ Node_{②} \end{array} \right] = \left[\begin{array}{ccc} 1 & 0 & 1 \\ 1 & 1 & 1 \end{array} \right] \tag{2}$$

2.2 Two analysis models with FEM

As we discussed above section (2.1), we developed analysis models as shown in Figs.2 and 3. The left model is for the asymmetric model, the right one is for the symmetric model. These setups are simulated for a typical satellite model. Cubes of each model indicate the main body component of satellites. The plates model solar array panels. Each model has a total of twenty-nine or thirty-two elements, respectively. In this research, the material properties are set as aluminum and details are shown in Appendix (7.1) [6]. As shown in this table, the length of one element for the asymmetric model is set at 0.35 [m], and set at 0.31 [m] for the symmetric model. Therefore, the total size of the asymmetric model is about 0.35 [m] (X direction) $\times$ 1.4 [m] (Y direction) $\times$ 0.70 [m] (Z direction). The symmetric model is 0.35 [m] (X direction) $\times$ 1.6 [m] (Y direction) $\times$ 0.62 [m] (Z direction). For the asymmetric model, we assumed that the body component mass is much heavier than the panel mass ($Mass_{body} >> Mass_{panel}$).

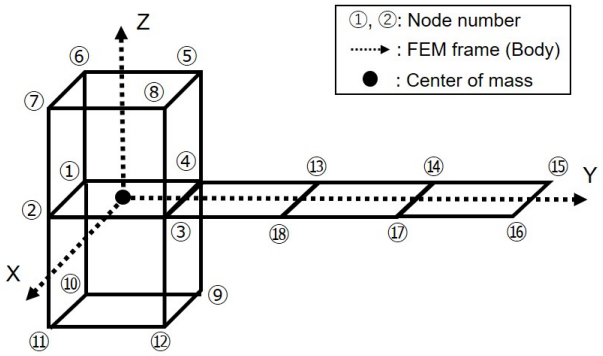

Fig. 2: Asymmetric model

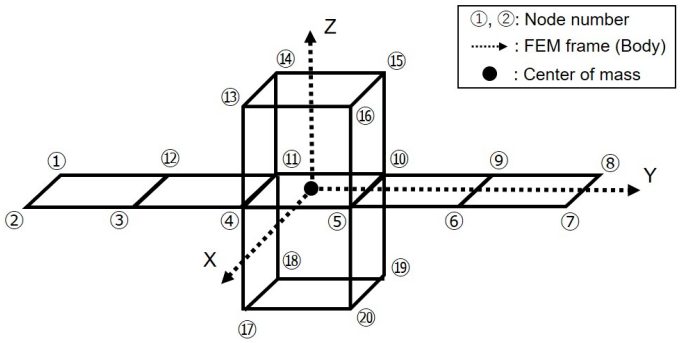

Fig. 3: Symmetric model

3. TUMBLING ANALYSIS

3.1 Dynamcal equation for FEM

To investigate system response with attenuation, the damping equation is used for simulation.

$$M\ddot{X} + C\dot{X} + KX = f(t) \tag{3}$$

where M is the mass matrix, C is the damping coefficient, K is the stiffness matrix, and the restoring force is KX by Hooke's law. The mass and stiffness matrix are developed by basic definition [5]. Details of the mass and stiffness matrix are developed in Appendix (7.2) . Excitation force $f(t)$ is a periodic acceleration matrix, which is shown in the following section. The damping equation is a second order differential equation and is modified into a first order equation with $X = X_1$, $\dot{X} = X_2$ as shown in Eq (4).

$$\begin{bmatrix} \dot{X}_1 \\ \dot{X}_2 \end{bmatrix} = \begin{bmatrix} 0 & 1 \\ -\frac{K}{M} & -\frac{C}{M} \end{bmatrix} \begin{bmatrix} X_1 \\ X_2 \end{bmatrix} + \begin{bmatrix} 0 \\ \frac{1}{M} \end{bmatrix} f(t) \tag{4}$$

For simulations with FEM, state X has three dimensional displacements and angles between them. Since one X has 6×1 size, total size of X can be $6N \times 1$ ($N = 1, 2, 3...$). N indicates the number of elements.

$$X = \begin{bmatrix} x_1 \\ x_2 \\ x_3 \\ \theta_1 \\ \theta_2 \\ \theta_3 \end{bmatrix} \tag{5}$$

3.2 Rotational acceleration matrix

To simulate model tumbling motion, rotational acceleration matrix is added as a time varying acceleration. The following equations presents the three dimensional acceleration matrices. Here, $\omega_\perp$ represents a perpendicular vector relative to ω_0. α indicates the ratio of the pure rotation and tumbling.

$$f(t) = \begin{bmatrix} \omega^2 - \omega_\perp^2 \cos^2(\omega_0 t) & -\omega_\perp^2 \sin(\omega_0 t)\cos(\omega_0 t) & -\omega_\perp \omega_0 \cos(\omega_0 t) \\ -\omega_\perp^2 \sin(\omega_0 t)\cos(\omega_0 t) & \omega^2 - \omega_\perp^2 \sin^2(\omega_0 t) & -\omega_\perp \omega_0 \sin(\omega_0 t) \\ -\omega_\perp \omega_0 \cos(\omega_0 t) & -\omega_\perp \omega_0 \sin(\omega_0 t) & \omega^2 - \omega_0^2 \end{bmatrix} \vec{r} \tag{6}$$

where, $\omega_0 = \frac{2\pi}{values}$, values are from 600, 1800, and 3600. $\omega_\perp = \alpha \times \omega_0$, $\omega^2 = \omega_0^2 + \omega_\perp^2$, $\vec{r}$ = node coordinate.

Fig.4 shows the exaggerated behavior of the asymmetric model tumbling. Fig.5 shows the symmetric model. Black lines indicate the nominal position and blues line stand for the displacement caused by deformation. Because the displacements are tiny, they are scaled to express deformation effectively. The acceleration force is applied to each center mass. Coordinate [0 0 0] is equivalent to the center of mass and origin.

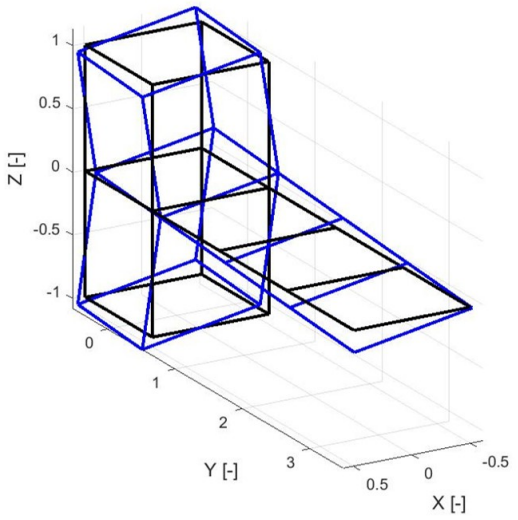

Fig. 4: The behavior of asymmetric model tumbling

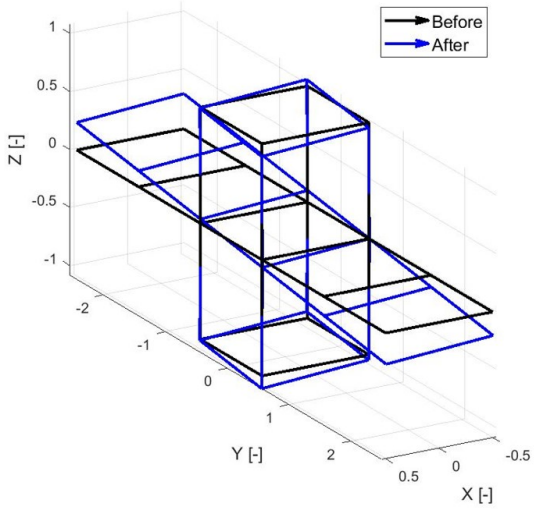

Fig. 5: The behavior of symmetric model tumbling

3.3 Results for tumbling analysis

Fig.6 to 9 show the displacement histories of each model. Each plot demonstrates the first node position (=Node ①). Although the rotational rate is $\frac{2\pi}{600}$ and α is 0.01, the model is tumbling.

Table 1: Parameters of tumbling simulation

C (Damping coefficient)	α	ω_0
0.1	0.01	$\frac{2\pi}{600}$

3.3.1 Tumbling for the asymmetric model

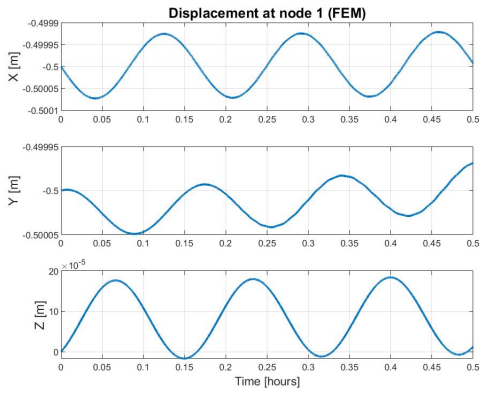

Fig. 6: Displacement for the asymmetric model

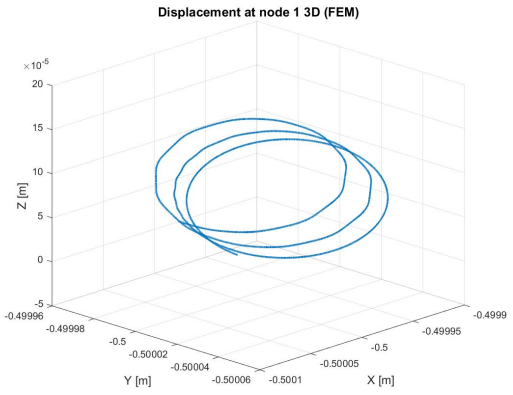

Fig. 7: 3D displacement for the asymmetric model

3.3.2 Tumbling for the symmetric model

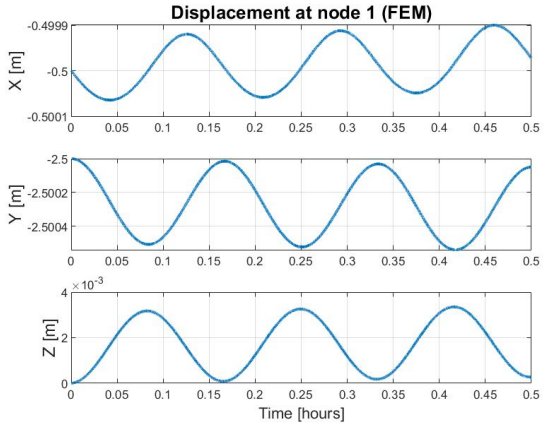

Fig. 8: Displacement for the symmetric model

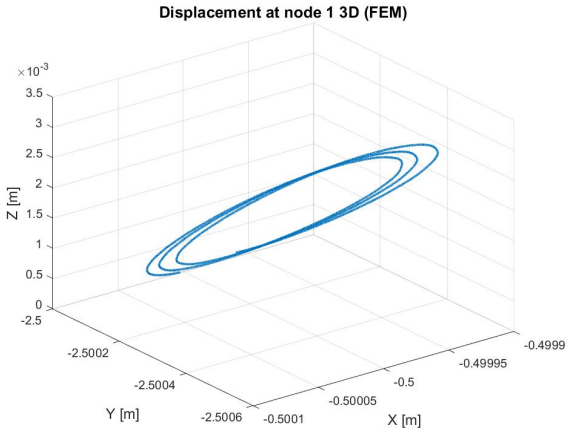

Fig. 9: 3D displacement for the symmetric model

4. BOUC-WEN MODEL WITH FEM ANALYSIS

4.1 Background

Modeling of damping structure is a very complex phenomenon, because many factors are related to damping and its energy dissipation. The factors of the energy loss are discussed in Lazan book [7]. The examples are friction, internal forces, size of the geometry, and temperature. One solution to analyze the level of the damping and the amount of energy loss is to determine the area within the hysteresis loop [8]. Hysteresis is also caused by magnetic and dielectric, viscous medium flow, thermoelastic, etc. The enveloping cycle is formed by two hysteresis curves with the loading and unloading processes with maximal amplitudes of variation [9].

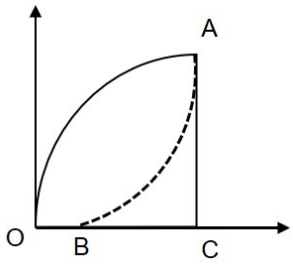

Fig. 10: Energy loss process

$$Energy\ loss = \triangle OAC - \triangle ABC \tag{7}$$

For structural dynamics, the hysteresis loop in Fig.10 is caused by the restoring force and structural deformation. The loop shape is often inelastic. The area enclosed by each loop is the amount of the energy dissipation over a cycle. The Bouc-Wen model is one of the most widely accepted model of hysteresis to describe the characteristics of nonlinear damping in a system. Bouc originally proposed this model [10], and it has been generalized by Wen [11] and other researchers. This model is composed of the restoring force and deformation through a nonlinear differential equation, which has unknown parameters. By changing these parameters, a large variety of different shapes of the hysteresis loops are generated [12].

As we discussed above, hysteresis is an important concept for energy loss. Hysteresis loops generated from only FEM simulation, which total restoring force is expressed by $F = Kx$, have complex shape shown in Figs.11 and 12. Fig.11 shows the asymmetric model, while Fig.12 is the symmetric model result. Because of this complexity, we simplify the system and calculate energy with the Bouc-Wen model. Total restoring force and displacements are summed overall nodes of each model.

$$Total\ Resotoring\ Force = \sum_{i=1}^{N} Kx_i,\ (i = 1,2,...N) \tag{8}$$

$$Total\ Displacement = \sum_{i=1}^{N} x_i,\ (i = 1,2,...N) \tag{9}$$

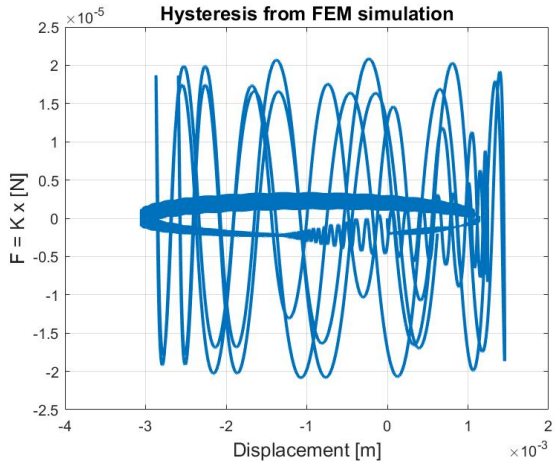

Fig. 11: Hysteresis by FEM for the asymmetric model

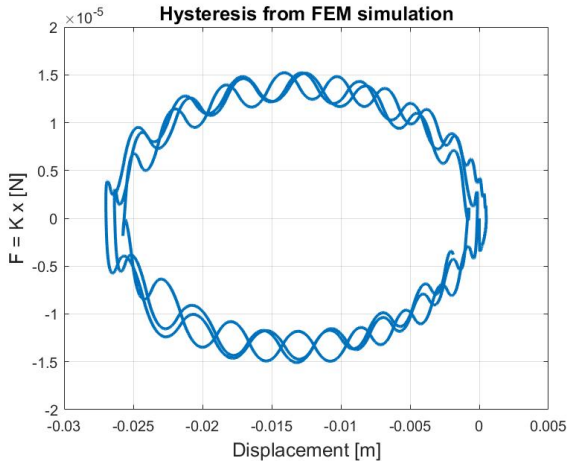

Fig. 12: Hysteresis by FEM for the symmetric model

4.2 Dynamical equations for hysteresis [13][14]

In this section, a mathematical formulation of the Bouc-Wen model is presented. As an example, for equation of motion of a single degree of freedom system:

$$m\ddot{x}(t) + c\dot{x} + F(t) = f(t) \tag{10}$$

where m is the mass, $x(t)$ is the displacement, c the damping coefficient, $F(t)$ is the restoring force, and $f(t)$ is the excitation force, the overdot is derivative with respect to time. It is assumed that the excitation force is cyclic. The Bouc-Wen model is described by the following differential equation:

$$\dot{g}(t) = A\dot{x}(t) - \beta|\dot{x}(t)||g(t)|^{n-1}g(t) - \gamma\dot{x}(t)|g(t)|^n \tag{11}$$

where g is an imaginary hysteretic displacement, $A(>0)$, γ and n are dimensionless quantities controlling the hysteresis shape and size. From the definition, n is integer and positive values, and β is a positive number.

4.2.1 Restoring force $F(t)$

The total restoring force $F(t)$ can be decomposed into an elastic and a hysteretic part as follows:

$$F^{el}(t) = aku(t),\ F^{h}(t) = (1-a)kg(t) \tag{12}$$

$$F(t) = aku(t) + (1-a)kg(t) \tag{13}$$

where k is the stiffness coefficient, and a $(0 < a < 1)$ is the ratio of post-yield to pre-yield (elastic). Superscripts indicate elastic and hysteretic. The restoring force is purely hysteretic if $a = 0$ and it is absolutely elastic if $a = 1$.

4.2.2 Parametaric constraints and criteria

The Bouc-Wen model has the unknown parameters (a, A, β, γ, and n), which are redundant. To remove this redundancy, A is set to one [15]. In addition, by using the constraints [16], the total number of unknown parameter is reduced.

$$\frac{A}{\beta + \gamma} = 1 \tag{14}$$

Table 2: Parameters of the differential model of hysteresis

Parameters	Description
a $(0 < a < 1)$	Ratio of linear to nonlinear response
$A(=1)$, β, γ, $(\beta + \gamma = 1)$	Hysteresis shape control
n	Sharpness of yield

4.3 Absorbed hysteretic energy

Absorbed hysteretic energy represents the energy loss by the hysteretic system, and is quantified as the area of the hysteretic force under the total displacement. Therefore, the absorbed hysteretic energy (per unit of mass) is defined as

$$\varepsilon(t) = (1-a)K \int_{x(0)}^{x(T)} g(t)dx = (1-a)k \int_0^T g(t)\dot{x}(t)dt \tag{15}$$

4.4 Dynamical equation for simulation

Eqs.(16) and (17) show the basic equation of motion for simulation with combined FEM dynamics and hysteretic. State X has position (r), velocity (v), and hysteretic parameter (g).

$$X = \begin{bmatrix} r \\ v \\ g \end{bmatrix} \tag{16}$$

$$\dot{X} = \begin{bmatrix} v \\ M^{-1}[f(t) - Cv - aKr - (1-a)Kg] \\ Av - \beta|v(t)||g(t)|^{n-1}g(t) - \gamma v(t)|g(t)|^n \end{bmatrix} \tag{17}$$

5. SIMULATION RESULTS

In order to investigate the absorbed energy of the different rotational rate, the hysteresis loop is simulated. By combining the FEM simulation and the Bouc-Wen model, the complex shape of the hysteresis loop is simplified and can predict the absorbed energy. The simulation results are shown in this section.

5.1 Simulation sequence

Fig.13 shows the sequence of the simulation which are combined with the FEM dynamics and the Boc-Wen model (Eq.(17)). Acceleration (tumbling) is applied into Eq.(17). From this simulation, elastic and hysteric force are evaluated with variation by a, which is the ratio of elastic and hysteric forces. The sum of the elastic and hysteric forces is equivalent to the total restoring force. Because the hysteresis shape is complex if the plots are taken only from FEM results, the force is simplified as a sinusoid. After fitting, this approximation function is used as the exciting force and goes into the damping equation which includes the Bouc-Wen model. This is the transition point from the multiple node system (FEM) to the simple system. By calculating the area of hysteresis plot, the energy loss of the system can be estimated.

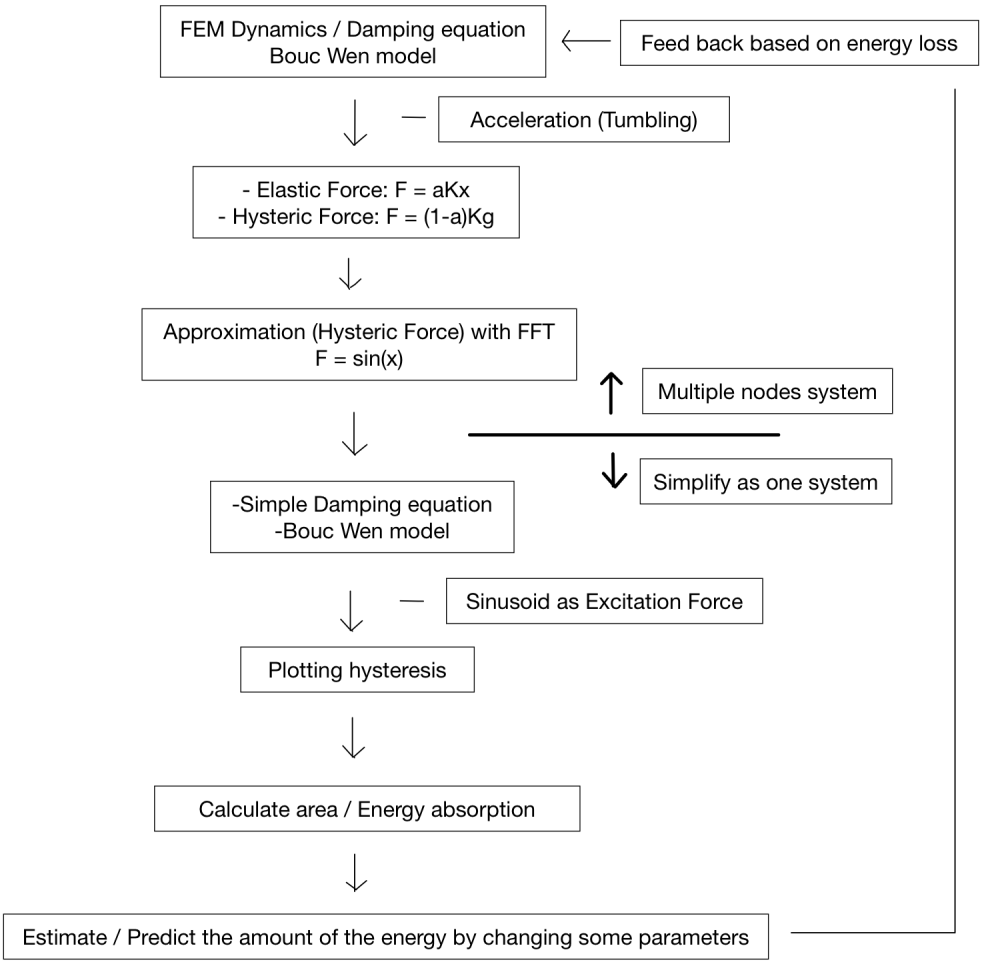

Fig. 13: Simulation sequence

5.2 Fast Fourier Transform (FFT) [17]

During the transformation from the FEM dynamics into a simple system, a Fast Fourier Transform is used as an approximation. It is assumed that $f(t)$ is defined for all real numbers t. For any $s \in R$, integrating $f(t)\ e^{-j\omega t}$ with respect to t produces a complex valued function of ω. Therefore, the fourier transform $F(\omega)$ is a complex valued function of $\omega \in R$.

$$F(\omega) = \int_{-\infty}^{\infty} f(t) e^{-j\omega t} dt \tag{18}$$

5.3 Simulation parameters

At first, we investigate the hysteresis shape by changing β from 1 to 20. γ is constrained appropriately. After calculating the hysteresis parameter, we compared absorbed energy with the change in rotational rate. We set up a as 0.5, meaning that elastic and hysteretic forces are equal. n is set to 1.

Table 3: Parameters for Bouc-Wen simulation

Parameters	Values
A	1
c (Damping)	0.1
α (ratio between the perpendicular and nominal)	0.01
ω_0	$\frac{2\pi}{600}$, $\frac{2\pi}{1800}$, $\frac{2\pi}{3600}$
β	1, 5, 10, 20
γ	1-β
$n\ (>=1)$	1
a	0.5

5.4 Simulation results for the asymmetric model

5.4.1 $\omega_0 = \frac{2\pi}{600}$

Calculation results are shown in this section. Fig.14 indicates the time history of the summed displacements and total restoring force. The right side of Fig.14 shows the variation of the FFT analysis, in which β varies from one to twenty. Its vertical axis is normalized by the maximum of amplitude, the horizontal axis is frequency. Due to beating, there are two peaks in this figure. The peak frequencies are almost exactly $\frac{1}{600} = 0.0017$ and $\frac{1}{60} = 0.0169$ [Hz]. Considering the force amplitude, the fitting function for $\omega_0 = \frac{2\pi}{600}$ is set as:

$$f(t) = 1.8 \times 10^{-5} \sin(\frac{2\pi}{60}t) + 5 \times 10^{-6} sin(\frac{2\pi}{600}t) \tag{19}$$

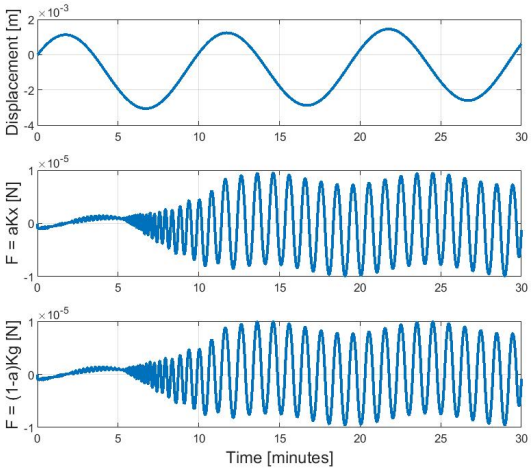

Fig. 14: Displacement and force history

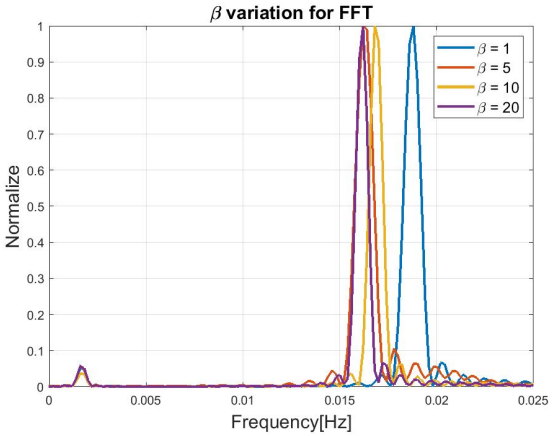

Fig. 15: FFT analysis with β change ($\frac{2\pi}{600}$)

Fig.16 shows the total restoring force and the fitting function. Using Eq.(19), the hysteresis of the Bouc-Wen model is generated and shown in Fig.18. During the transition from multiple node system to the simple system, K_{system} is also evaluated to generate a simple hysteresis loop. From Fig.17, K_{system} is estimated at 0.01 as a maximum value. m_{system} is taken from the total mass of system. Figs.16 and 17 are based on $\beta = 10$.

$$K_{system} = \frac{\sum_{i=1}^{N} F_i}{\sum_{i=1}^{N} x_i} \ (i = 1, 2, ..., N) \tag{20}$$

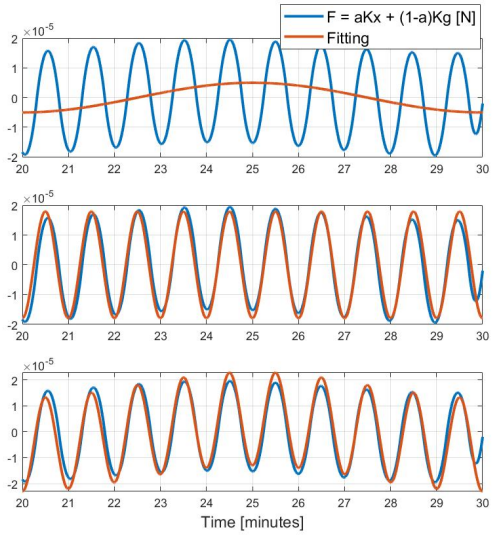

Fig. 16: Fitting function for the asymmetric model

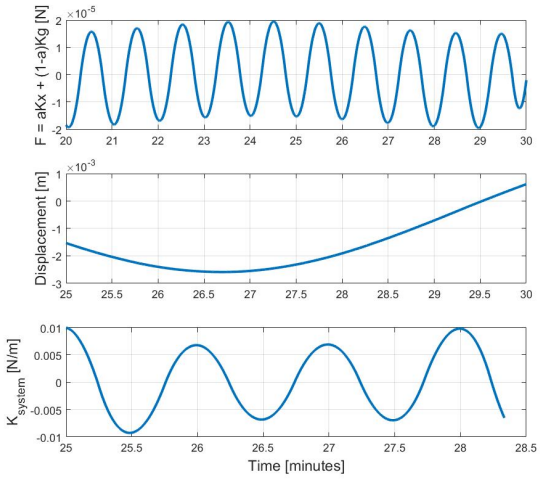

Fig. 17: K_{system} for the asymmetric model

Then, using the fitting function (Eq.19), K_{system}, and m_{system}, hysteresis is generated and shown in Fig.18. The fitting function is scaled by 10^2 to express the hysteresis loop clearly. The β value is changed from one to twenty. Increasing β increases the width of the loop. Fig.19 indicates the hysteresis, which is divided into each period with β = 10. The period is about 60 [sec]. Considering these results, absorbed energy is calculated for many periods, which is shown in Fig.20.

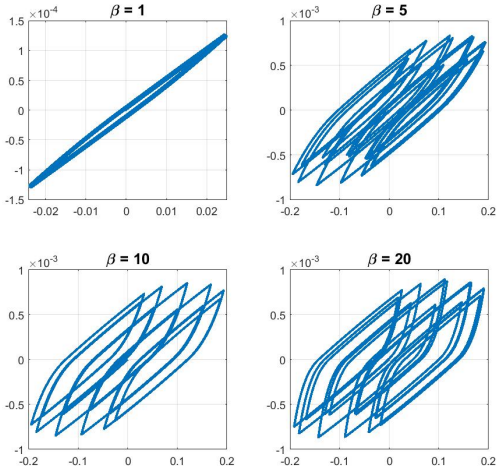

Fig. 18: Hysteresis for $\frac{2\pi}{600}$

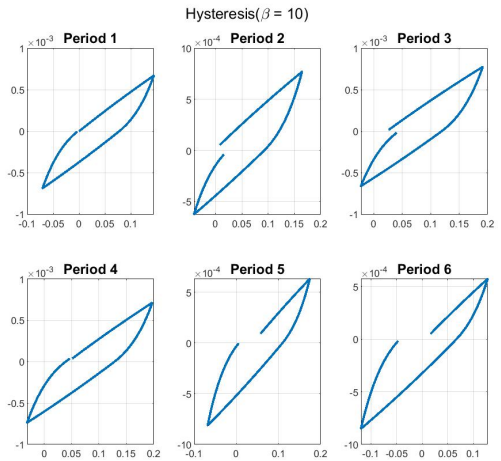

Fig. 19: Divided hysteresis for $\frac{2\pi}{600}$

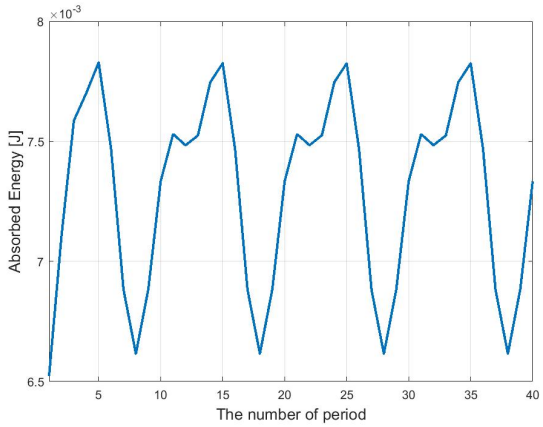

Fig. 20: Absorbed energy for $\frac{2\pi}{600}$ ($\beta = 10$)

5.4.2 $\omega_0 = \frac{2\pi}{1800}$ and $\frac{2\pi}{3600}$

Based on the same process as the previous section, we simulated the different rotational rate. Then its absorbed energy was compared. As the spin rates increase, the FFT becomes simpler. At the same time, the fitting function becomes also simple. Fig.22 shows the total restoring force and the fitting function. The rotational rate is $\frac{2\pi}{1800}$, the peak is 0.004 [Hz]. Then the fitting function is set as following:

$$f(t) = 7 \times 10^{-5} \sin(\frac{2\pi}{250} t) \tag{21}$$

Again, using total restoring force and displacements, K_{system} is estimated as 0.1. Hysteresis plots are shown in Fig.23 and 24 ($\beta = 10$).

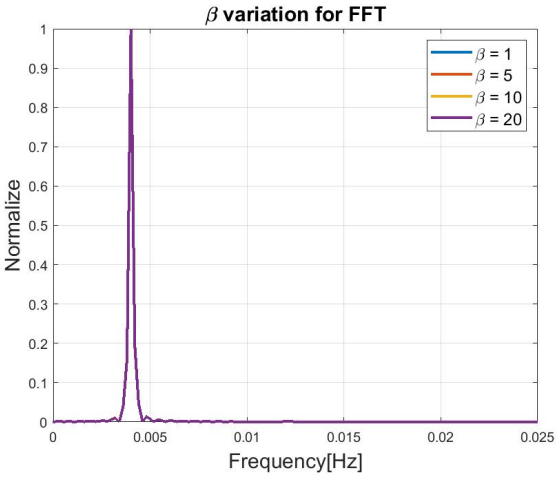

Fig. 21: FFT analysis with β change ($\frac{2\pi}{1800}$)

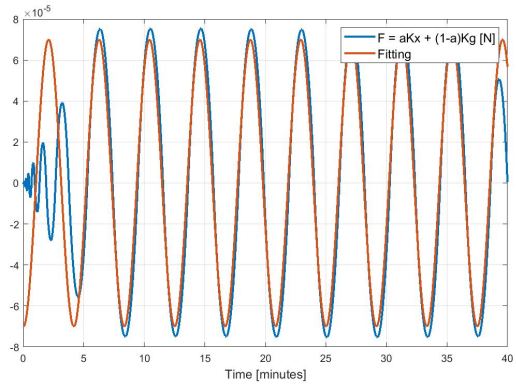

Fig. 22: Fitting function for the asymmetric model

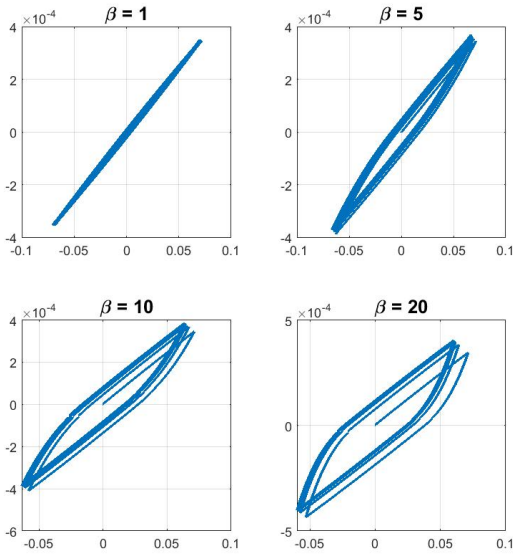

Fig. 23: Hysteresis for $\frac{2\pi}{1800}$

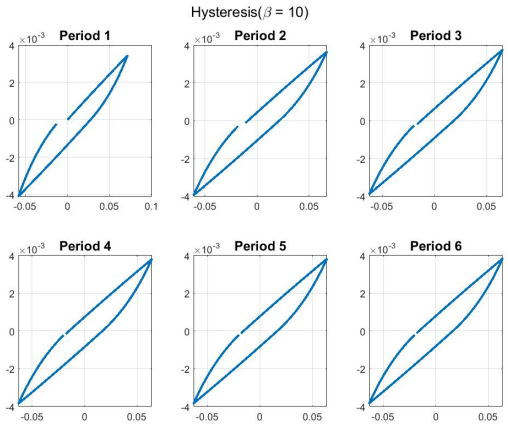

Fig. 24: Divided hysteresis for $\frac{2\pi}{1800}$ ($\beta = 10$)

For $\omega_0 = \frac{2\pi}{3600}$, the fitting function is calculated with Eq.(22), because the peak of FFT analysis is 0.002 [Hz] = $\frac{1}{480}$. The FFT result is shown in Fig. 25. K_{system} is estimated as 0.1.

$$f(t) = 2 \times 10^{-6} \sin(\frac{2\pi}{480} t) \tag{22}$$

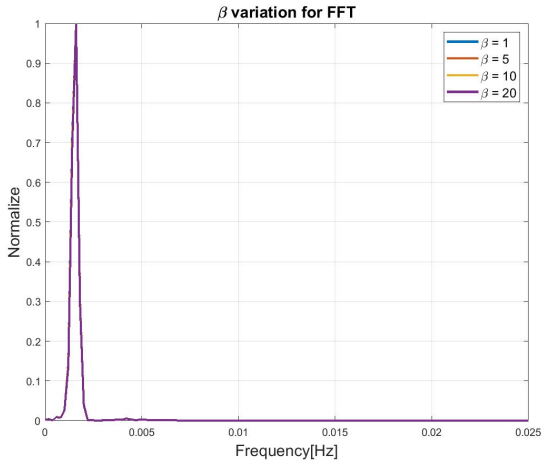

Fig. 25: FFT analysis with β change ($\frac{2\pi}{3600}$)

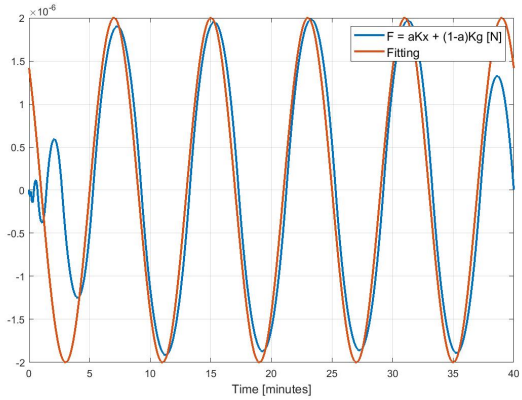

Fig. 26: Fitting function for asymmetric model

5.5 Energy comparison for the asymmetric model

Fig.27 shows the relationship between the absorbed energy and the rotational rate, holding $\beta = 10$. Higher rotational rate leasd to much more absorbed energy than lower rotational rates. In addition, the energy decays exponentially as the rotational rate gets slower.

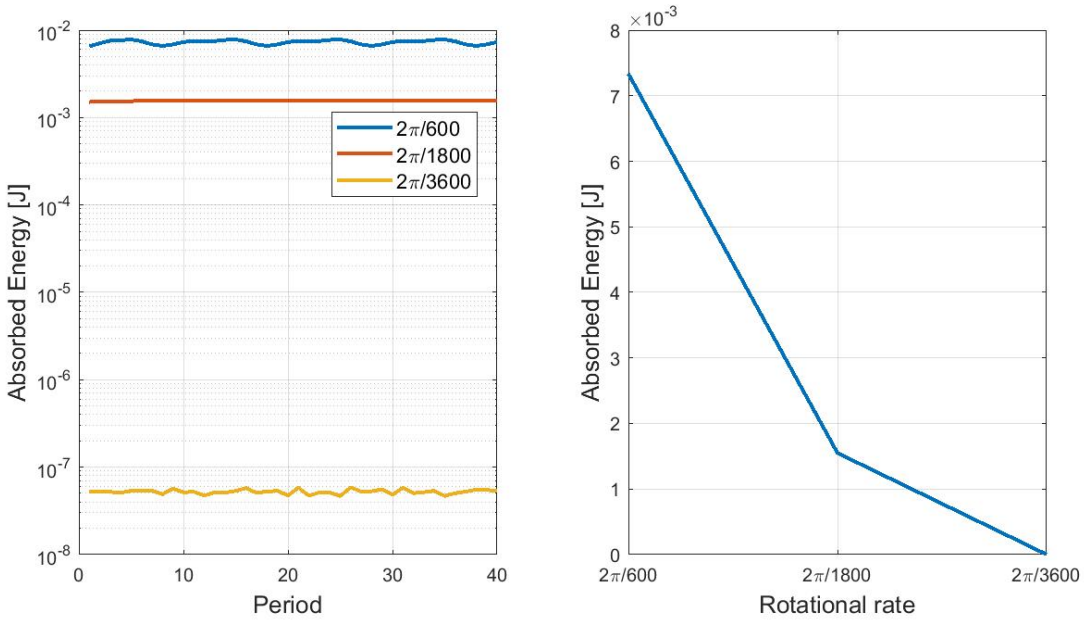

Fig. 27: Energy comparison for the asymmetric model (β = 10)

5.6 Energy comparison for the symmetric model

We also analyzed the absorbed energy for the symmetric model with the change of the spin rate. Fitting functions and K_{system} are shown below. From the top to bottom, $\omega_0 = \frac{2\pi}{600}$, $\frac{2\pi}{1800}$, and $\frac{2\pi}{3600}$. β is set as 5. Fig.28 shows the relationship between the spin rate and the absorbed energy. As in the asymmetric model model simulation, high spin rate leads to much more absorbed energy than slower rotation. Absorbed energy decays exponentially with spin rate.

$\frac{2\pi}{600}$

$$f(t) = 1.5 \times 10^{-5} \sin(\frac{2\pi}{600}t) + 1 \times 10^{-5} \sin(\frac{2\pi}{35}t),\ K_{system} = 0.01 \tag{23}$$

$\frac{2\pi}{1800}$

$$f(t) = 4 \times 10^{-5} \sin(\frac{2\pi}{120}t),\ K_{system} = 0.03 \tag{24}$$

$\frac{2\pi}{3600}$

$$f(t) = 2.5 \times 10^{-5} \sin(\frac{2\pi}{350}t),\ K_{system} = 0.03 \tag{25}$$

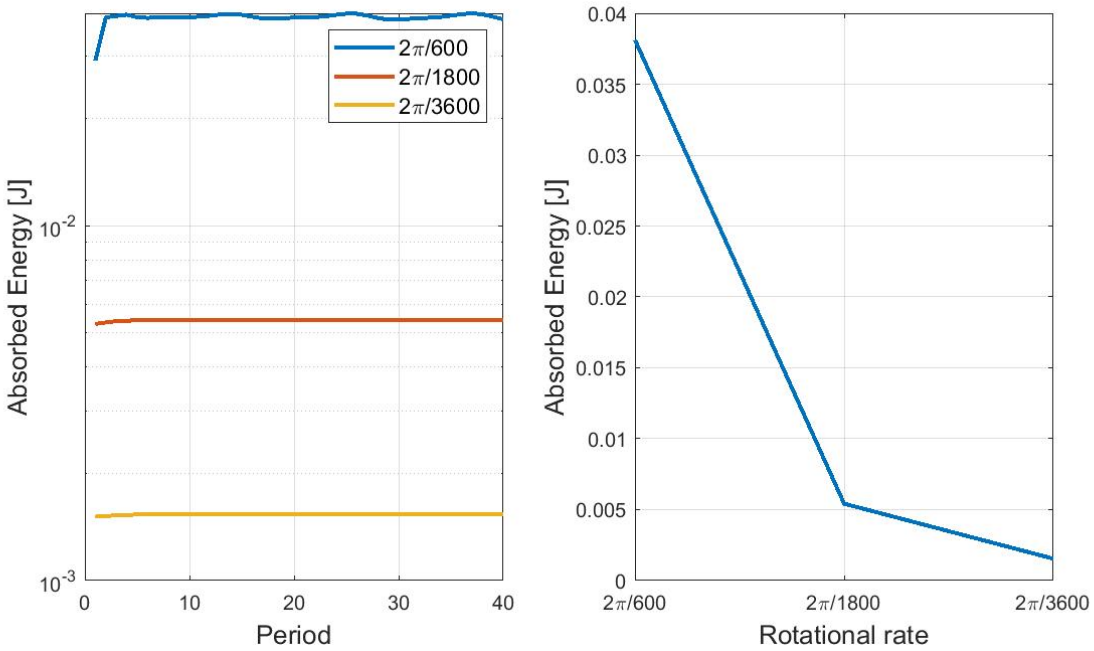

Fig. 28: Energy comparison for the symmetric model ($\beta = 5$)

6. CONCLUSION

By combing FEM dynamics with the Bouc-Wen model, we investigated the relationship between rotational rates and energy dissipation. Section 2 described the theoretical basis of FEM simulation of defunct satellite and the two analysis models to be used. Section 3 presented a tumbling simulation with the damping equation and two analysis models. Section 4 provided the Bouc-Wen model and a derivation for the combination of FEM and the Bouc-Wen. In section 5, we presented the numerical results of the arbitrary hysteresis parameters and energy loss. Various hysteresis parameters and rotational rates have been analyzed. The exponential relationship between the absorbed energies, the rotational rates, and the hysteresis parameters was revealed. Also, numerical simulations for two models showed similar tendencies for energy decay. We believe that these modeling techniques will be useful in studying the detumbling satellites or asteroids. These analyses simplify full FEM simulations into hysteretic dynamics with the Bouc-Wen model. In addition, hysteretic parameters are chosen arbitrary from infinite options. To precisely estimate and predict the rotation state and the energy dissipation, more consideration should be give to parameters selection. Finally, a way of feeding back from energy loss to evolving simulation is needed.

7. APPENDIX

7.1 Parameters of structural model

Table 4: Parameters of structural model

Parameters	Value
Length of an element: L[m]	One panel model: 0.35, Symmetric model: 0.31
Thickness [m]	0.002
Width [m]	0.02
Density [kg/m^3]	2857.4
Modulus of elasticity [GPa]	70.0
Transverse modulus of elasticity [GPa]	28.0

7.2 Mass and stiffness matrix

For mass matrix for FEM dynamics is given by,

$$[M] = \frac{\rho AL}{420}\begin{bmatrix} 140 & 0 & 0 & 0 & 0 & 0 & 70 & 0 & 0 & 0 & 0 & 0 \\ 0 & 156 & 0 & 0 & 0 & 22L & 0 & 54 & 0 & 0 & 0 & -13L \\ 0 & 0 & 156 & 0 & -22L & 0 & 0 & 0 & 54 & 0 & 13L & 0 \\ 0 & 0 & 0 & 140I_p/A & 0 & 0 & 0 & 0 & 0 & 70I_p/A & 0 & 0 \\ 0 & 0 & -22L & 0 & 4L^2 & 0 & 0 & 0 & -13L & 0 & -3L^2 & 0 \\ 0 & 22L & 0 & 0 & 0 & 4L^2 & 0 & 13L & 0 & 0 & 0 & -3L^2 \\ 70 & 0 & 0 & 0 & 0 & 0 & 140 & 0 & 0 & 0 & 0 & 0 \\ 0 & 54 & 0 & 0 & 0 & 13L & 0 & 156 & 0 & 0 & 0 & -22L \\ 0 & 0 & 54 & 0 & -13L & 0 & 0 & 0 & 156 & 0 & 22L & 0 \\ 0 & 0 & 0 & 70I_p/A & 0 & 0 & 0 & 0 & 0 & 140I_p/A & 0 & 0 \\ 0 & 0 & 13L & 0 & -3L^2 & 0 & 0 & 0 & 22L & 0 & 4L^2 & 0 \\ 0 & -13L & 0 & 0 & 0 & -3L^2 & 0 & -22L & 0 & 0 & 0 & 4L^2 \end{bmatrix} \tag{26}$$

For stiffness matrix for FEM dynamics is given by,

$$[K] = \begin{bmatrix} \frac{EA}{L} & 0 & 0 & 0 & 0 & 0 & -\frac{EA}{L} & 0 & 0 & 0 & 0 & 0 \\ 0 & \frac{12EI_z}{L^3} & 0 & 0 & 0 & \frac{6EI_z}{L^2} & 0 & -\frac{12EI_z}{L^3} & 0 & 0 & 0 & \frac{6EI_z}{L^2} \\ 0 & 0 & \frac{12EI_y}{L^3} & 0 & -\frac{6EI_y}{L^2} & 0 & 0 & 0 & -\frac{12EI_y}{L^3} & 0 & -\frac{6EI_y}{L^2} & 0 \\ 0 & 0 & 0 & \frac{GJ}{L} & 0 & 0 & 0 & 0 & 0 & -\frac{GJ}{L} & 0 & 0 \\ 0 & 0 & -\frac{6EI_y}{L^2} & 0 & \frac{4EI_y}{L} & 0 & 0 & 0 & \frac{6EI_y}{L^2} & 0 & \frac{2EI_y}{L} & 0 \\ 0 & \frac{6EI_y}{L^2} & 0 & 0 & 0 & \frac{4EI_z}{L} & 0 & -\frac{6EI_z}{L^2} & 0 & 0 & 0 & \frac{2EI_z}{L} \\ -\frac{EA}{L} & 0 & 0 & 0 & 0 & 0 & \frac{EA}{L} & 0 & 0 & 0 & 0 & 0 \\ 0 & -\frac{12EI_z}{L^3} & 0 & 0 & 0 & -\frac{6EI_z}{L^2} & 0 & \frac{12EI_z}{L^3} & 0 & 0 & 0 & -\frac{6EI_z}{L^2} \\ 0 & 0 & -\frac{12EI_y}{L^3} & 0 & \frac{6EI_y}{L^2} & 0 & 0 & 0 & \frac{12EI_y}{L^3} & 0 & \frac{6EI_y}{L^2} & 0 \\ 0 & 0 & 0 & -\frac{GJ}{L} & 0 & 0 & 0 & 0 & 0 & \frac{GJ}{L} & 0 & 0 \\ 0 & 0 & -\frac{6EI_y}{L^2} & 0 & \frac{2EI_y}{L} & 0 & 0 & 0 & \frac{6EI_y}{L^2} & 0 & \frac{4EI_y}{L} & 0 \\ 0 & \frac{6EI_z}{L^2} & 0 & 0 & 0 & \frac{2EI_z}{L} & 0 & -\frac{6EI_z}{L^2} & 0 & 0 & 0 & \frac{4EI_z}{L} \end{bmatrix} \tag{27}$$

where ρ is density, A is cross-sectional area, L is total length, E is young's modules, G is shear modulus, J is area moment of inertia, $I_{x,y,z}$ are moment of inertia and I_p is polar moment of inertia.

8. REFERENCES

[1] R. C. W. R. A. Albuja, D.J. Scheeres and E. Ryan., "The YORP effect on the GOES 8 and GOES 10 satellites: A case study," *Advances in Space Research*, vol. 61, pp. 122–144, 2018.

[2] P. P. V. D. B. H. T. P. M. J. G. A. I. M. I. J. K. P. Lowry. S., Fitzsimmons. A., "Direct detection of the asteroidal YORP effect," *Science*, vol. 316, pp. 272–274, 2007.

[3] T. S. Kojima. Y. and O. Y., "Dynamic simulation of stick-slip motion of a flexible solar array," *Control Engineering Practice*, vol. 16, pp. 724–735, 2008.

[4] P. M. a. A. B. A.M. Solovyov., M.E. Semonov., "Bouc-wen model of hysteretic damping," in *3rd International Conference Information Technology and Nanotechnology*, 25-27 April 2017.

[5] K. K., *Mechanical structure vibration engineering (in Japanese)*. Morikita Publishing Co., Ltd, Tokyo, Japan, 2012.

[6] T. H. Sakamoto. R. and O. Y., "Improvement of deployment repeatability by the vibration produced by macro fiber composite actuator," *Bulletin of the JSME Mechanical Engineering Letters*, vol. 2, no. 16, pp. 1–8, 2016.

[7] L. B. J, *Damping of materials and members in structural mechanics*. Oxford Pergamon Press, 1968.

[8] F. Orban., "Damping of materials and members in structures," in *5th International Workshop on Multi-Rate Processes and Hysteresis (MURPHYS 2010)*, 2010.

[9] A. N. Danilin, "Vibrations of mechanical systems with energy dissipation hysteresis," *Mechanics of Solids*, vol. 52, no. 3, pp. 254–265, 2017.

[10] R. Bouc., "Forced vibration of mechanical systems with hysteresis," in *Proceedings of the 4th Conference on Nonlinear Oscillations,*, p. 315, Prague, Czechoslovakia,1967.

[11] Y. K. Wen, "Method for random vibration of hysteretic systems," *Journal of the Engineering Mechanics Division*, vol. 102, no. 2, pp. 249–263, 1976.

[12] A. B. G. C. F. F. Ma., H. Zhang. and P. Paevere., "Parameter analysis of the differential model of hysteresis," *Journal of Applied Mechanics*, vol. 71, no. 3, pp. 342–349, 2004.

[13] S. S. C. M. Chang. and M. Terzo., "Modelling of hysteresis in vibration control systems by means of the bouc-wen model," *Shock of Vibration*, vol. 2016, 2016.

[14] O. Vinogradov. and I. Pivovarov., "Vibrations of a system with non-linear hysteresis," *Journal of Sound and Vibration*, vol. 111, no. 3, pp. 145–152, 1986.

[15] T. T. Baber. and Y. K. Wen., "Random vibration of hysteretic degrading systems," *Journal of the Engineering Mechanics Division*, vol. 107, no. 6, pp. 1069–1087, 1981.

[16] M. C. Constantinou. and M. A. Adnane., *Dynamics of soil-baseisolated structure systems: evaluation of two models for yielding systems*. Department of Civil Engineering, Drexel University, 1987.

[17] B. G. Osgood., *Lectures on the Fourier Transform and Its Applications*. American Mathematical Society, 2019.